# Surface Chemical Compositions and Dispersity of Starch Nanocrystals Formed by Sulfuric and Hydrochloric Acid Hydrolysis

Benxi Wei[1,2], Xueming Xu[1,2], Zhengyu Jin[1,2]*, Yaoqi Tian[1,2]*

1 The State Key Laboratory of Food Science and Technology, School of Food Science and Technology, Jiangnan University, Wuxi, China, 2 Synergetic Innovation Center of Food Safety and Nutrition, Jiangnan University, Wuxi, China

## Abstract

Surface chemical compositions of starch nanocrystals (SNC) prepared using sulfuric acid ($H_2SO_4$) and hydrochloric acid (HCl) hydrolysis were analyzed by X-ray photoelectron spectroscopy (XPS) and FT-IR. The results showed that carboxyl groups and sulfate esters were presented in SNC after hydrolysis with $H_2SO_4$, while no sulfate esters were detected in SNC during HCl-hydrolysis. TEM results showed that, compared to $H_2SO_4$-hydrolyzed sample, a wider size distribution of SNC prepared by HCl-hydrolysis were observed. Zeta-potentials were −23.1 and −5.02 mV for $H_2SO_4$- and HCl-hydrolyzed SNC suspensions at pH 6.5, respectively. Nevertheless, the zeta-potential values decreased to −32.3 and −10.2 mV as the dispersion pH was adjusted to 10.6. After placed 48 h at pH 10.6, zeta-potential increased to −24.1 mV for $H_2SO_4$-hydrolyzed SNC, while no change was detected for HCl-hydrolyzed one. The higher zeta-potential and relative small particle distribution of SNC caused more stable suspensions compared to HCl-hydrolyzed sample.

## Introduction

Recently, there has been growing interest in starch nanocrystals (SNC) for abundant availability of starch, comparatively easy processability, biocompatibility, biodegradability, and non-toxicity, comparing with inorganic nanoparticles [1]. These properties make them as excellent candidates for implant materials and drug carriers. SNC have been also used as good reinforcing fillers in natural rubber, pullulan, polyurethane, polyvinyl alcohol, and soybean protein [2]. Furthermore, considering that the size of SNC is generally <100 nm (at least in one dimension) and SNC is readily surface-modified to obtain different hydrophobility [3,4], SNC and their derivatives are deemed to be used as high-efficiency nanoparticle emulsifiers to prepare Pickering emulsions [5].

SNC are crystalline platelets resulting from the disruption of the semi-crystalline structure of starch granules by hydrolysis of amorphous parts. The preparation methods by different acid hydrolysis have been extensively studied [6–8]. At present, SNC are obtained generally by treating starch slurry with dilute sulfuric acid ($H_2SO_4$) or hydrochloric acid (HCl) at 25–55°C for various periods of time. However, hydrolysis of starch by $H_2SO_4$ was more widely adapted because of its high efficiency comparing with HCl [9,10]. Furthermore, it was reported that SNC derived from $H_2SO_4$ hydrolysis resulted in more stable suspensions than HCl hydrolyzed samples [11]. This better stability was attributed to the surface chemical compositions of SNC, which reflected the interaction behaviors among SNC in aqueous or organic solvents.

A homogeneous dispersion state of SNC was a key step required for high mechanical performances of rubber or other material properties [12]. The electrostatic repulsive forces could also significantly affect the properties of Pickering emulsions [13]. Therefore, the surface chemical compositions of SNC played an important role in the application of different fields. So far, the change of surface chemical compositions of SNC after acid hydrolysis and the mechanism for better stability of SNC suspensions derived from $H_2SO_4$ have not been explicitly reported except for some hypotheses. These proposals mainly included the formation of sulfate ester groups on the surface of the SNC [9], the surface compositions of starch (such as lipids, protein and other metal ions carried by starch) making starch suspensions charge-stabilized [14], acquisition of more stable starch suspension after treating with high pressure homogenization due to higher zeta-potential of the colloids [15], and a stable and uniform SNC aqueous suspension prepared by introducing negative charges using crosslinking modification by sodium hexametaphosphate [16]. It could be concluded that the repulsive forces (expressed as zeta-potential) caused by surface chemical groups affected the dispersity of SNC.

In this work, the change of surface chemical compositions of SNC after $H_2SO_4$- and HCl- hydrolysis was, thus, analyzed and its effects on zeta-potentials of SNC suspensions were examined. This will provide basic information of SNC hydrolyzed with HCl and $H_2SO_4$ and explain the reason of their different dispersity.

## Materials and Methods

### Materials and Reagents

Waxy maize starch (WMS) was kindly donated by Tianjin Tingfung Starch Development Co., Ltd. (Tianjin, CHN). $H_2SO_4$, HCl, sodium hydroxide (NaOH), potassium chloride (KCl) and uranyl acetate were purchased from Sinopharm Chemical Reagent Co., Ltd. (Suzhou, CHN) and of analytical grade. Potassium bromide (KBr) was of spectroscopic grade and bought from Sinopharm Chemical Reagent Co., Ltd. (Suzhou, CHN). Milli-q water was used in all experiments.

### Preparation of Starch Nanocrystals

SNC were prepared by acid hydrolysis of waxy maize starch according to the method by Angellier et al. with minor modification [9]. Starch powders (50 g) were mixed with 500 mL of 3.16 M $H_2SO_4$ solution and placed at 40°C for 3 and 7 d under stirring at the speed of 200 rpm. For the HCl-hydrolyzed SNC, 20 g starch powders were mixed with 400 mL 2.2 N hydrochloric acid solution at 40°C for 7 d with constantly stirring at the speed of 200 rpm. The suspensions were washed by successive centrifugations in distilled water until pH was constant. The resultant suspensions were redispersed using Ultra Turrax T20 (IKA) at 13,500 rpm for 3 min to avoid aggregates and stored at 4°C with several drops of chloroform. The SNC concentrations were determined by weighting freeze-dried powders of the homogeneous dispersion of SNC (10 mL) and expressed as weight percentage relative to the volume of the water phase. The concentrations of $H_2SO_4$- and HCl-hydrolyzed SNC suspensions were 3.50% (w/v) and 2.08% (w/v), respectively. Different concentrations of SNC suspensions were derived by diluting the "stock" homogeneous dispersion of SNC.

### X-ray Photoelectron Spectroscopy (XPS) Analysis of SNC

XPS experiments were carried out by means of a Multifunctional imaging electron spectrometer (Thermo ESCALAB 250XI, USA). The spectrometer was equipped with a monochromatic Al Kα ($hv = 1486.6$ eV) X-ray source of 150 W at 15 kV. The kinetic energy of photoelectrons was determined with a hemispheric analyzer set to pass energy of 160 eV for wide-scan spectra and 20 eV for high-resolution spectra, respectively. During all measurements, electrostatic charging of the samples was avoided by means of a low-energy electron source working in combination with a magnetic immersion lens. Later, all recorded peaks were shifted by the same value to set the C1s peak to 284.8 eV. Quantitative elemental compositions were determined from peak areas using sensitivity factors experimentally and the spectrometer transmission function. Spectrum background was subtracted according to Shirley [17]. The high-resolved spectra were deconvoluted by means of a computer routine. Peaks were fitted to Gaussian-Lorentzian ratio (8:2) curves after subtraction of baseline (Shirley method). SNC used for XPS analysis were lyophilized powders.

### Fourier Transform Infrared Spectroscopy (FT-IR) of SNC

The FT-IR spectra of the lyophilized and HCl- and $H_2SO_4$-hydrolyzed (for 3 d and 7 d) SNC powders were collected between 4000 cm$^{-1}$ and 500 cm$^{-1}$ on a FT-IR spectrophotometer (5DXC FT-IR, Nicolet Co. US) with 256 scans at a resolution of 4 cm$^{-1}$. The SNC powders (3 mg) were ground with spectroscopic grade KBr (200 mg) powders and then pressed into 1 mm pellets. A blank disc was used as the background.

### Measurement of Zeta-Potentials of HCl- and $H_2SO_4$-hydrolyzed SNC Suspension

Zeta-potentials were determined in presence of 1 mM KCl at 25°C using a commercial Malvern Zetasizer Nano ZS 90. The pH of the suspension (0.01%, w/v) was adjusted using dilute HCl or NaOH. The SNC suspensions were placed for 2 h and 48 h before measurement. Measurements were carried out in quintuplicate for error analysis. The refractive index of fluid and particle used were 1.33 and 1.53, respectively.

### Transmission Electron Microscope (TEM)

TEM observations were performed using a JEOL JEM-2100 (HR) at an acceleration voltage of 80 kV. SNC suspensions (0.01%, w/v, pH = 6.5) hydrolyzed by HCl and $H_2SO_4$ were sonicated at 4°C for 15 min. A drop of suspension was spread onto the copper grids coated with carbon support film. Prior to complete drying, a drop of 2% (w/v) uranyl acetate negative stain was added. After 1 min, the liquid in excess was blotted with filter paper and the remaining film was allowed to dry for observation.

### Statistical Analysis

Statistical analysis was performed using ORIGIN 7.5 (OriginLab Inc., USA). Data were expressed as means ± standard deviations and analyzed by a one-way analysis of variance (ANOVA). P value ≤0.05 was regarded as significant throughout the study.

## Results and Discussion

### Surface Chemical Compositions of SNC

The general XPS spectra of WMS and $H_2SO_4$-hydrolyzed starch for 3 d (SNC$_{H2SO4,3}$) and 7 d (SNC$_{H2SO4,7}$) were displayed in Fig. 1. The peaks around 531, 400, 285, and 168 eV were consisted with oxygen, nitrogen, carbon, and sulfur atoms, respectively. The elemental surface composition (%) and the oxygen-to-carbon ratios of the different samples were summarized in Table 1. For WMS, the oxygen/carbon (O/C) ratio was 0.43, which was lower than the theoretical O/C ratio (0.83). This indicated that the surface of WMS was composed of considerable amounts of other components except of polysaccharide. According to previous reports, the high carbon content was resulted from the surface lipids, because 0.08%–0.14% surface lipids (mainly free fatty acids) were presented in native waxy maize starch granules. Surface lipids were non-starch lipids in the cereal endosperm that strongly adsorbed to the surface layers of the starch granules during starch isolation [18,19]. This demonstrated that surface lipids were the hydrocarbon impurities with strong adsorption behavior reported in previous studies [3,20,21]. Small amounts of nitrogen atoms were detected in the WMS due to the protein presented on the surface, which was in agreement with the report of Rindlav-Westling & Gatenholm [22]. With the hydrolysis process extending, the O/C ratio of SNC$_{H2SO4,3}$ did not show significant change in the first 3 d, whereas it increased from 0.43 to 0.61 after hydrolysis for 7 d. The relative slow increase of O/C ratio in the first 3 days might result from the incomplete exposed internal reducing ends, since waxy maize starch could not absolutely crack. As the hydrolysis process extending, more and more internal reducing ends were exposed, leading to the increase of the O/C ratio. However, no significant changes of O/C ratio were detected between $H_2SO_4$- and HCl-prepared samples after hydrolyzing for 7 d.

XPS spectra of SNC$_{H2SO4,7}$ showed that the peak intensity corresponding to oxygen atoms became almost two times higher than the one corresponding to carbon atoms. This increase
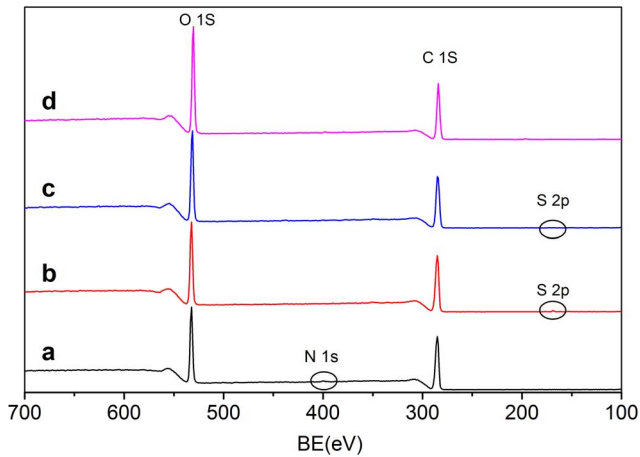
**Figure 1. General XPS spectra of (a) WMS, (b) SNC$_{H2SO4,3}$, (c) SNC$_{H2SO4,7}$, and (d) SNC$_{HCl,7}$.**
doi:10.1371/journal.pone.0086024.g001

indicated the disruption of starch granules and the increase of reducing ends. The surface lipids that washed away by acid hydrolysis were contributed to the relative increase of oxygen atoms [3]. Small amounts of sulfur atoms were introduced to the surface of SNC after hydrolysis with H$_2$SO$_4$. No surface nitrogen was observed after acid hydrolysis, this result was in agreement with the findings reported by Thielemans, et al [23].

## Deconvolution of C 1 s and S 2p Peaks

The C 1 s peak in the XPS spectra was deconvoluted for each sample into several peaks (Fig. 2). The different binding energies and relative percentages of the peaks were summarized in Table 2. For WMS, the C 1 s signal revealed four peaks at 284.8, 286.3,

**Table 1.** Elemental surface composition (atomic %) and oxygen to carbon ratio of starch, HCl- and H$_2$SO$_4$-hydrolyzed SNC.

| Samples | O | C | S | N | O/C |
|---------|------|------|------|------|------|
| WMS | 30.08 | 69.30 | - | 0.52 | 0.43 |
| SNC$_{H2SO4,3}$ | 31.04 | 68.82 | 0.14 | - | 0.45 |
| SNC$_{H2SO4,7}$ | 37.70 | 62.23 | 0.07 | - | 0.61 |
| SNC$_{HCl,7}$ | 38.66 | 61.34 | - | - | 0.63 |

doi:10.1371/journal.pone.0086024.t001

287.6, and 288.9 eV arising from C1 (carbon atoms bonded only to carbon and/or hydrogen atom (C-C/C-H)), C2 (carbon atoms bonded to a single oxygen atom (C-O)), C3 (carbon atoms bonded to two noncarbonyl oxygen atoms or to a single carbonyl oxygen atom (O-C-O/C = O)), and C4 (carbon atoms bonded with a single oxygen atom and with a carbonyl oxygen (O-C = O)), respectively. The presence of C-C/C-H and O-C = O bonds further confirmed the lipids on the surface of WMS. After hydrolysis for 3 d, the relative content of C4 peak increased from 1.32% for WMS to 4.27% for SNC$_{H2SO4,3}$, and the relative content of C1 peak decreased simultaneously. The increase in C4 peak might be ascribed to the adsorption of formic and levulinic acids derived from the hydrolyzed products of glucose [24,25]. Formic acid had higher adsorption capacity and stronger affinity than levulinic acid [26]. Therefore, the increase of C4 peak (O-C = O) might mainly result from the adsorption of formic acid. The relative content of C4 peak decreased to 3.18% with the hydrolyzed time extending to 7 d. This may be due to an equilibrium adsorption state of organic acids and the complete removal of surface lipids during the hydrolysis process. These results were accorded with the previous report, in which carboxyl
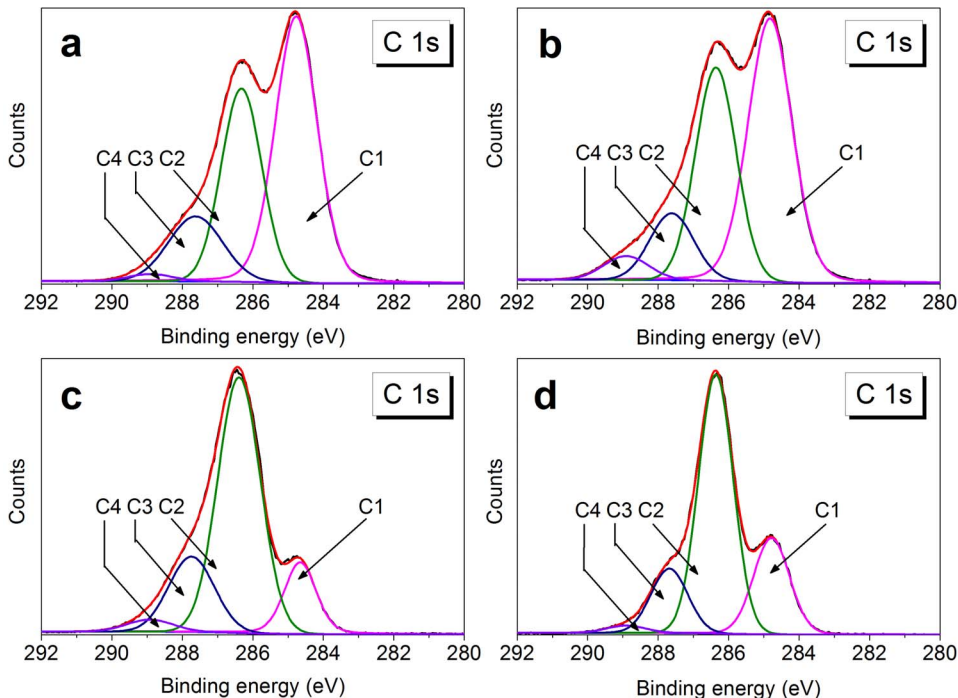


**Figure 2. The high-resolution C 1 s deconvoluted XPS spectra of (a) WMS, (b) SNC$_{H2SO4,3}$, (c) SNC$_{H2SO4,7}$, (d) SNC$_{HCl,7}$.**
doi:10.1371/journal.pone.0086024.g002

**Table 2.** Surface functional group composition as obtained from the deconvolution of the C 1 s signal.

| Samples | C1 | C2 | C3 | C4 |
|---|---|---|---|---|
| | C-C/C-H | C-O | O-C-O/C = O | O-C = O |
| BE (eV)[a] | 284.8 | 286.3±0.1 | 287.6±0.1 | 288.9±0.05 |
| WMS | 50.42 | 33.29 | 14.97 | 1.32 |
| SNC$_{H2SO4,3}$ | 49.23 | 34.94 | 11.56 | 4.27 |
| SNC$_{H2SO4,7}$ | 14.57 | 62.54 | 19.71 | 3.18 |
| SNC$_{HCl,7}$ | 23.60 | 59.10 | 15.49 | 1.83 |

[a]The binding energy for each signal is given with variation seen between different sample.
doi:10.1371/journal.pone.0086024.t002

groups were detected in $H_2SO_4$-hydrolyzed cellulose microcrystal suspensions [27]. The relative content of C4 peak for SNC$_{HCl,7}$ was lower than that for SNC$_{H2SO4,7}$, the reason is probably that the concentration of $H_2SO_4$ used in the experiment was much higher than that of HCl.
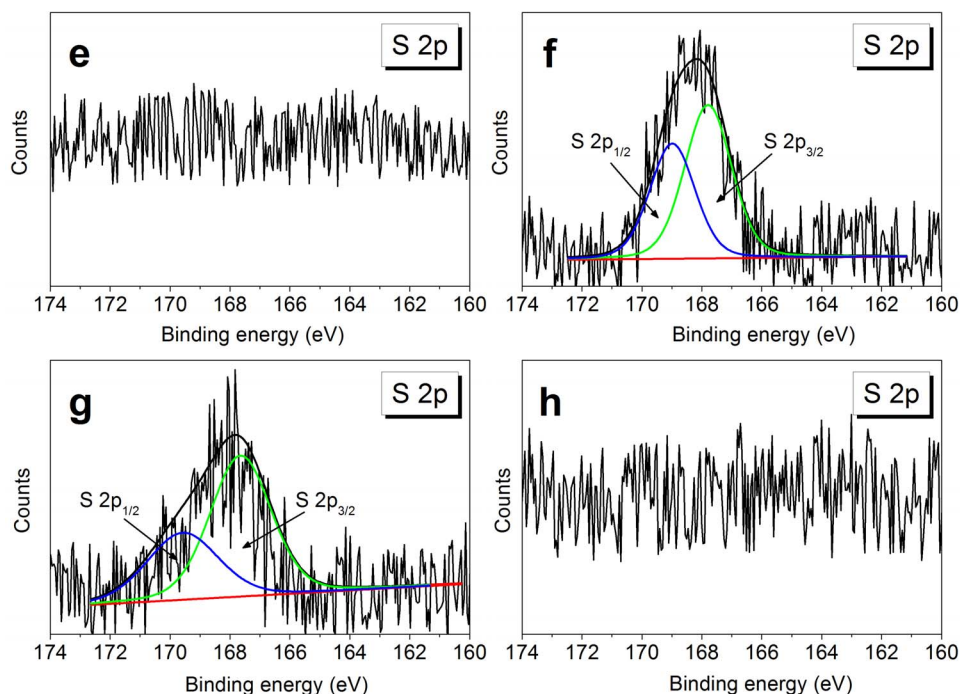
The high resolution S 2p peaks of WMS, SNC$_{H2SO4,3}$, SNC$_{H2SO4,7}$, and SNC$_{HCl,7}$ were shown in Fig. 3. No surface sulfur was detected in WMS and SNC$_{HCl,7}$. However, it was detected for SNC$_{H2SO4,3}$ and SNC$_{H2SO4,7}$ samples. The S 2p spectra at 168 eV were composed of S 2p3/2 and S 2p1/2 peaks, and both peaks represented sulfur in its highest oxidation state, i.e., $O-SO_3^-$ or $C-SO_3^-$. Nevertheless, no C-S bond was presented in the C 1 s peaks for SNC$_{H2SO4,3}$ and SNC$_{H2SO4,7}$ (Figs. 2b/c), indicating sulfate esterification of hydroxyl bonds and $H_2SO_4$ (Figs. 3f/g). The formation of sulfate esters was previously reported for cellulose nanocrystals, while the details were not shown for SNC except for some hypothesis [9,28]. The relative atomic percentages of sulfur reduced from 0.14% for SNC$_{H2SO4,3}$ to

0.07% for SNC$_{H2SO4,7}$. This decrease indicated that sulfate esters were probably hydrolyzed with the hydrolyzed process extending.

## FT-IR Analysis of SNC

Fig. 4 illustrated FT-IR spectra of waxy maize starch and HCl- and $H_2SO_4$-hydrolyzed SNC. For WMS (Fig. 4a), a typical spectrum enclosed absorption bands at 3435 cm$^{-1}$, revealing the O-H stretching vibration of -OH groups in the glucose units, and the peaks at 2929 cm$^{-1}$, 1450 cm$^{-1}$ and 1370 cm$^{-1}$ ascribe to the C-H stretching and bending modes of the methylene. The peak at 1648 cm$^{-1}$ originated from the bending vibration of H-O-H in the absorbed $H_2O$. The peaks at 1155 cm$^{-1}$, 1080 cm$^{-1}$, and 1020 cm$^{-1}$ reflected the stretching mode of C-O-C linkages in the glucosidic rings [29]. For the HCl- and $H_2SO_4$-hydrolyzed SNC, the emergence of two new bands adsorbing at 1560 cm$^{-1}$ and 1340 cm$^{-1}$ could be ascribed to the asymmetric and symmetric stretching of -COOH. The adsorbing bands shifted to lower wavenumbers compared to previous reports [30]. This difference was probably because of hydrocarbon chain effect from levulinic acid lowed the adsorbing band of carboxylate groups [31], and the resulted adsorbing peaks at 1560 and 1340 cm$^{-1}$ were overlapped of formic and levulinic acids. As the hydrogen bonds were formed between carboxylate groups and SNC, which reduced the adsorbing bands of carboxylate groups [32]. Therefore, the present band at 1644 cm$^{-1}$ might be a combination of carbonyl groups and absorbed $H_2O$ [33]. It was obvious that the band at 1644 cm$^{-1}$ for WMS was considerably narrower than HCl- and $H_2SO_4$-hydrolyzed samples, which confirmed the interaction of carbonyl groups and -OH through hydrogen bonds. These results suggested that formic and levulinic acids were adsorbed on the surface of SNC.

In addition, the band at 862 cm$^{-1}$ for SNC$_{H2SO4,7}$ was stronger than that of the other samples, indicated that an overlapping band existed in the region of 823 cm$^{-1}$–881 cm$^{-1}$ (Fig. 4c). The overlapping band could be assigned to the vibration of C-O-S



**Figure 3. The high-resolution S 2p deconvoluted XPS spectra of (e) WMS, (f) SNC$_{H2SO4,3}$, (g) SNC$_{H2SO4,7}$, and (h) SNC$_{HCl,7}$.**
doi:10.1371/journal.pone.0086024.g003
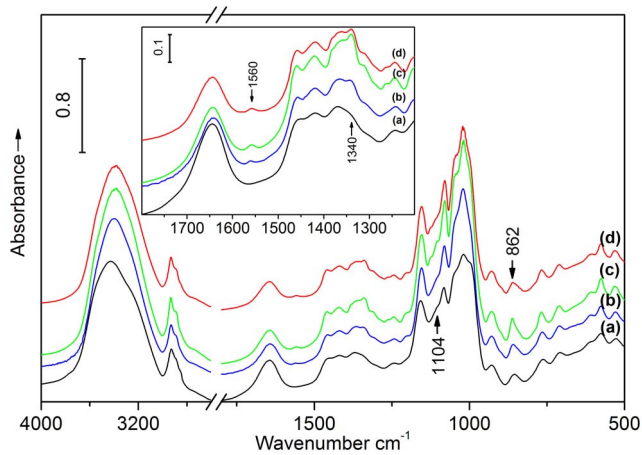
**Figure 4. FT-IR spectra of (a) WMS, (b) SNC_{H2SO4,3}, (c) SNC_{H2SO4,7}, and (d) SNC_{HCl,7}.**
doi:10.1371/journal.pone.0086024.g004

bond, which was in a good agreement with values reported in the literature [34]. Otherwise, the slight increase of the adsorbing band at $1104$ cm$^{-1}$ attributed to sulfate also proved possibility of the formation of sulfate ester.

## Reactions Occurred During Acid Hydrolysis

According to the above analysis, it could be concluded that three major reactions occurred during acid hydrolyzed process. (1)

Breakage of α-D-(1-4) and α-D-(1-6)-glycosidic bonds was the dominant reaction, which resulted in disappearance of amorphous and semicrystalline layers of the WMS, leaving the acid-resistant fraction named SNC; (2) Glucose was further degraded to formic and levulinic acids, and adsorption of these acids to the surface of SNC made them negative-charged (Fig. 5); (3) Formation of sulfate ester groups on the surface of the SNC, and the esterification reaction occurred simultaneously with the hydrolysis of the sulfate ester.

## Zeta Potential of H$_2$SO$_4$- and HCl-hydrolyzed SNC Suspensions

Zeta-potentials of SNC$_{HCl,7}$ and SNC$_{H2SO4,7}$ suspensions at pH 6.5 and 10.6 placed for 2 and 48 h were shown in Fig. 6. For the SNC$_{HCl,7}$ suspension, the final pH was 6.5 with complete washing by distilled water. However, it was difficult to wash SNC$_{H2SO4,7}$ till neutrality due to presence of carboxyl groups and sulfate esters (Fig. 5). Therefore, the dispersion pH of SNC$_{H2SO4,7}$ suspension was adjusted to 6.5 with dilute NaOH in this work. Owing to the presence of sulfate esters and carboxyl groups, zeta-potential of SNC$_{H2SO4,7}$ reached $-23.1$ mV, which was much lower than that of the SNC$_{HCl,7}$ suspension. No changes of zeta-potentials were detected for the two samples after 48 h at pH 6.5. Zeta-potentials decreased to $-32.3$ and $-10.2$ mV for SNC$_{H2SO4,7}$ and SNC$_{HCl,7}$, respectively, while the dispersion pH was adjusted to 10.6 and placed for 2 h. After 48 h, zeta-potential for SNC$_{H2SO4,7}$ increased to $-24.1$ mV, while no changes were found for SNC$_{HCl,7}$. These results revealed that degradation of
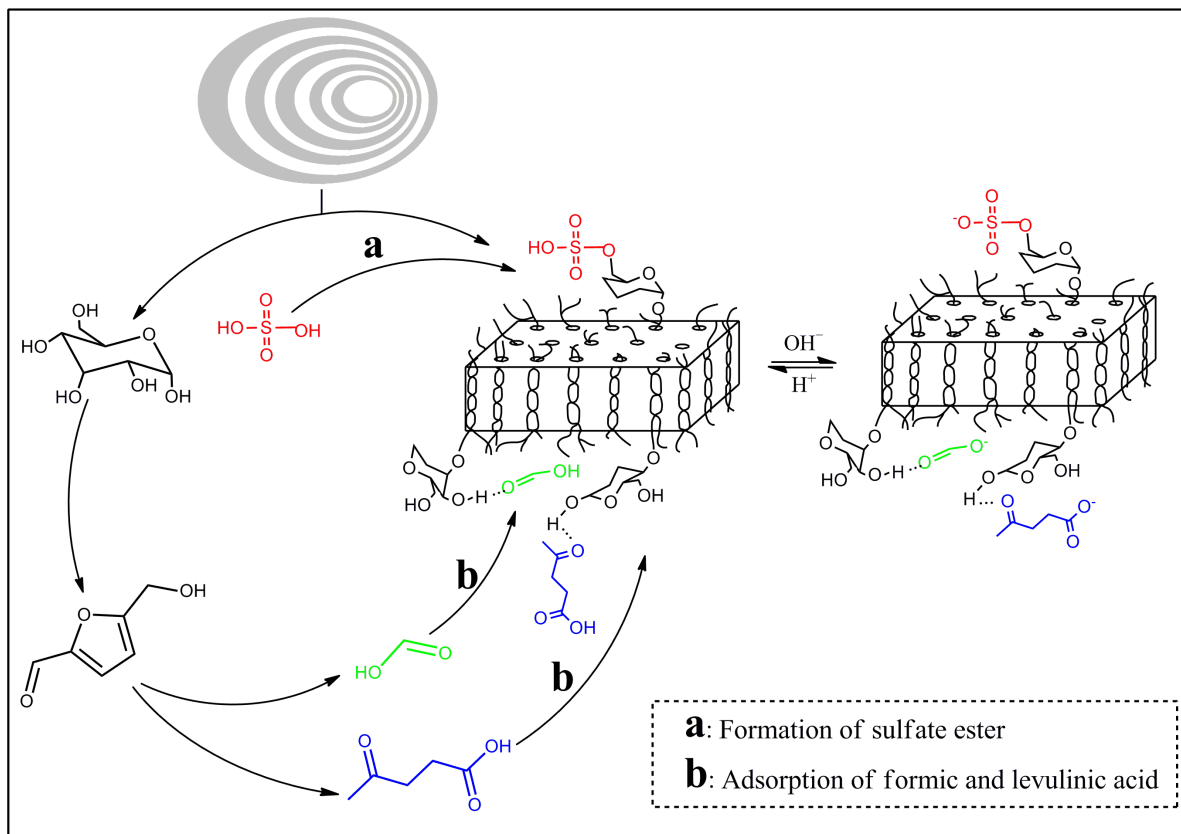


**Figure 5. Formation of sulfate esters and adsorption of formic and levulinic acids on the surface of SNC (a: Formation of sulfate ester, b: adsorption of formic and levulinic acids).**
doi:10.1371/journal.pone.0086024.g005
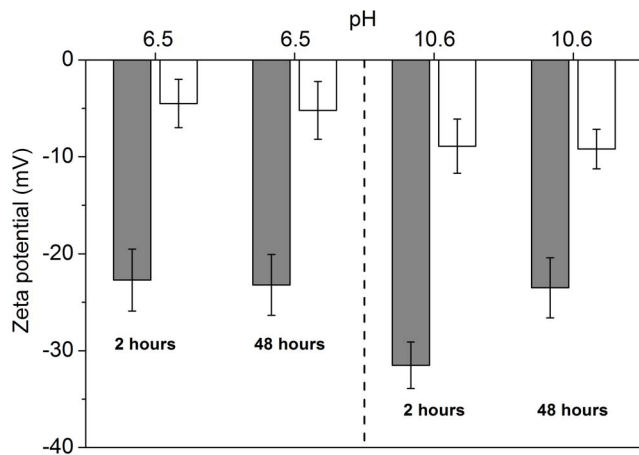
**Figure 6. Zeta potential of SNC$_{H2SO4,7}$ (gray color) and SNC$_{HCl,7}$ (white color) suspensions at pH 6.5 and 10.6 placed for 2 h and 48 h, respectively.** Data are represented as the mean $\pm$ standard deviation (n = 3).
doi:10.1371/journal.pone.0086024.g006

sulfate esters under alkaline condition contributed to the increase of the zeta-potential of SNC$_{H2SO4,7}$ suspension.

## TEM and Sedimentation Properties of HCl- and H$_2$SO$_4$-hydrolyzed SNC Suspensions

Fig. 7 shows TEM pictures and sedimentation properties of HCl- and H$_2$SO$_4$-hydrolyzed SNC suspensions. It could be seen from the picture that SNC derived from HCl-hydrolysis for 7 d showed a wide particle distribution, which was in the range of 50–300 nm. The low acid concentration used in the experiment might result in the heterogeneous SNC distribution. On the contrary, a homogenous SNC distribution in the range of 50–150 nm was obtained after H$_2$SO$_4$-hydrolysis for 7 d.
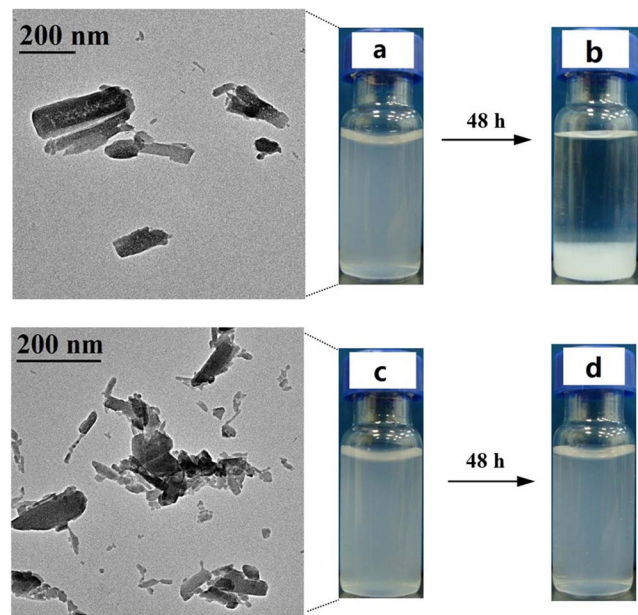
In addition, the aggregation behavior of HCl-hydrolyzed SNC was more serious than H$_2$SO$_4$-hydrolyzed sample. This could be ascribed to the relatively low zeta-potential of SNC suspension obtained by HCl-hydrolysis. Compared to the SNC$_{HCl,7}$ suspension, the higher zeta-potentials and the relative smaller particle distribution of SNC$_{H2SO4,7}$ generated the more stable suspensions.

## Conclusions

Surface chemical compositions of H$_2$SO$_4$-hydrolyzed SNC were different from the HCl-hydrolyzed samples. Adsorption of formic



**Figure 7. TEM pictures and sedimentation properties of HCl (a and b) and H$_2$SO$_4$ (c and d) hydrolyzed SNC suspensions after 2 h and 48 h.**
doi:10.1371/journal.pone.0086024.g007

and levulinic acids forming from the acid hydrolysis of glucose were probably contributed to the presence of carboxyl groups in HCl- and H$_2$SO$_4$-hydrolyzed SNC, while sulfate esters in H$_2$SO$_4$-hydrolyzed SNC were derived from the esterification reaction between hydroxyl bonds and H$_2$SO$_4$. The higher zeta potential for SNC$_{H2SO4,7}$ and the samller particle distribution limited flocculation and generated more stable suspensions comparing with the HCl-hydrolyzed sample. These results suggested that a more stable suspension was obtained by H$_2$SO$_4$-hydrolysis due to the higher zeta potential and much smaller and narrower particle size distribution.

## Author Contributions

Conceived and designed the experiments: BW YT. Performed the experiments: BW. Analyzed the data: BW XX YT. Contributed reagents/materials/analysis tools: XX ZJ YT. Wrote the manuscript: BW ZJ YT.

## References

1. Lin N, Huang J, Dufresne A (2012) Preparation, properties and applications of polysaccharide nanocrystals in advanced functional nanomaterials: a review. Nanoscale 4: 3274–3294.
2. Le Corre D, Bras J, Dufresne A (2010) Starch nanoparticles: a review. Biomacromolecules 11: 1139–1153.
3. Angellier H, Molina-Boisseau S, Belgacem MN, Dufresne A (2005) Surface chemical modification of waxy maize starch nanocrystals. Langmuir 21: 2425–2433.
4. Namazi H, Dadkhah A (2010) Convenient method for preparation of hydrophobically modified starch nanocrystals with using fatty acids. Carbohyd Polym 79: 731–737.
5. Li C, Sun P, Yang C (2012) Emulsion stabilized by starch nanocrystals. Starch-Stärke 497–502.
6. Kim HY, Lee JH, Kim JY, Lim WJ, Lim ST (2012) Characterization of nanoparticles prepared by acid hydrolysis of various starches. Starch-Stärke 64: 367–373.
7. Singh V, Ali S (2000) Acid degradation of starch. The effect of acid and starch type. Carbohyd Polym 41: 191–195.
8. Singh V, Ali S (2008) Properties of starches modified by different acids. Int J Food Prop 11: 495–507.
9. Angellier H, Choisnard L, Molina-Boisseau S, Ozil P, Dufresne A (2004) Optimization of the preparation of aqueous suspensions of waxy maize starch nanocrystals using a response surface methodology. Biomacromolecules 5: 1545–1551.
10. Chen G, Wei M, Chen J, Huang J, Dufresne A, et al. (2008) Simultaneous reinforcing and toughening: new nanocomposites of waterborne polyurethane filled with low loading level of starch nanocrystals. Polym 49: 1860–1870.
11. Angellier H, Putaux JL, Molina-Boisseau S, Dupeyre D, Dufresne A (2005) Starch nanocrystal fillers in an acrylic polymer matrix. Macromol Symp 221: 95–104.
12. Dufresne A (2008) Polysaccharide nano crystal reinforced nanocomposites. Can J Chem 86: 484–494.
13. Yang F, Niu Q, Lan Q, Sun D (2007) Effect of dispersion pH on the formation and stability of Pickering emulsions stabilized by layered double hydroxides particles. J Colloid Interf Sci 306: 285–295.
14. Marsh R, Waight S (1982) The effect of pH on the zeta potential of wheat and potato starch. Starch-Stärke 34: 149–152.

15. Liu D, Wu Q, Chen H, Chang PR (2009) Transitional properties of starch colloid with particle size reduction from micro-to nanometer. J Colloid and Interf Sci 339: 117–124.

16. Ren L, Jiang M, Zhou J, Tong J (2012) A method for improving dispersion of starch nanocrystals in water through crosslinking modification with sodium hexametaphosphate. Carbohyd Polym 87: 1874–1876.

17. Bratskaya S, Marinin D, Simon F, Synytska A, Zschoche S, et al. (2007) Adhesion and viability of two enterococcal strains on covalently grafted chitosan and chitosan/κ-carrageenan multilayers. Biomacromolecules 8: 2960–2968.

18. Morrison WR (1981) Starch lipids: A reappraisal. Starch-Stärke 33: 408–410.

19. Morrison WR (1988) Lipids in cereal starches: A review. J Cereal Sci 8: 1–15.

20. Dorris GM, Gray DG (1978) The surface analysis of paper and wood fibers by Esca-electron spectroscopy for chemical analysis-I. Applications to cellulose and lignin. Cell Chem Technol 12: 9–23.

21. Mjöberg P (1981) Chemical surface analysis of wood fibers by means of ESCA. Cell Chem Technol 15: 481–486.

22. Rindlav-Westling Å, Gatenholm P (2003) Surface composition and morphology of starch, amylose, and amylopectin films. Biomacromolecules 4: 166–172.

23. Putseys J, Lamberts L, Delcour J (2010) Amylose-inclusion complexes: Formation, identity and physico-chemical properties. J Cereal Sci 51: 238–247.

24. Mednick M (1962) The Acid-Base-Catalyzed Conversion of Aldohexose into 5-(Hydroxymethyl)-2-furfural2. J Org Chem 27: 398–403.

25. Mosier NS, Ladisch CM, Ladisch MR (2002) Characterization of acid catalytic domains for cellulose hydrolysis and glucose degradation. Biotechnol Bioeng 79: 610–618.

26. Liu BJ, Hu ZJ, Ren QL (2009) Single-component and competitive adsorption of levulinic/formic acids on basic polymeric adsorbents. Colloid Surfaces A 339: 185–191.

27. Araki J, Wada M, Kuga S, Okano T (1998) Flow properties of microcrystalline cellulose suspension prepared by acid treatment of native cellulose. Colloids Surfaces A 142: 75–82.

28. Roman M, Winter WT (2004) Effect of sulfate groups from sulfuric acid hydrolysis on the thermal degradation behavior of bacterial cellulose. Biomacromolecules 5: 1671–1677.

29. Sugama T (1997) Oxidized potato-starch films as primer coatings of aluminium. J Mater sci 32: 3995–4003.

30. Millar GJ, Rochester CH, Waugh KC (1995) An FTIR study of the adsorption of formic acid and formaldehyde on potassium-promoted Cu/SiO2 catalysts. J Catal 155: 52–58.

31. Ibrahim M, Nada A, Kamal DE (2005) Density functional theory and FTIR spectroscopic study of carboxyl group. Indian J Pure Ap Phy 44: 911–917.

32. Rivero S, García MA, Pinotti A (2011) Heat treatment to modify the structural and physical properties of chitosan-based films. J Agr Food Chem 60: 492–499.

33. Coleman MM, Skrovanek DJ, Hu J, Painter PC (1988) Hydrogen bonding in polymer blends. 1. FTIR studies of urethane-ether blends. Macromolecules 21: 59–65.

34. Koshy KM, Boggs JM (1997) The effect of anomerism and hydration on the COS vibrational frequency of D-galactose-3-sulfate determined by FTIR spectroscopy. Carbohyd Res 297: 93–99.